Photochemical & Photobiological Sciences

Cite this: DOI: 10.1039/c2pp25224d

www.rsc.org/pps

PAPER

A theoretical study of thionine: spin–orbit coupling and intersystem crossing†

Angela Rodriguez-Serrano,[a,b] Vidisha Rai-Constapel,[b] Martha C. Daza,[a] Markus Doerr[a,c] and Christel M. Marian*[b]

Received 28th June 2012, Accepted 24th July 2012
DOI: 10.1039/c2pp25224d

A study of the possible intersystem crossing (ISC) mechanisms (S ⇝ T) in thionine (3,7-diamino-phenothiazin-5-ium), which is conducive to the efficient population of the triplet manifold, is presented. The radiationless deactivation channels {S_1,S_2($\pi \rightarrow \pi^*$) ⇝ T_1,T_2($\pi \rightarrow \pi^*$)} have been examined. Since the direct ISC does not explain the high triplet quantum yield in this system, attention has been centered on the vibronic spin–orbit coupling between the low-lying singlet and triplet ($\pi \rightarrow \pi^*$) states of interest. An efficient population transfer from the $S_1(\pi_H \rightarrow \pi_L^*)$ state to the $T_2(\pi_{H-1} \rightarrow \pi_L^*)$ state *via* this channel is confirmed. The calculated ISC rate constant for this channel is $k_{ISC} \approx 3.35 \times 10^8$ s^{-1}, which can compete with the radiative depopulation of the $S_1(\pi_H \rightarrow \pi_L^*)$ state *via* fluorescence ($k_F \approx 1.66 \times 10^8$ s^{-1}) in a vacuum. The $S_1(\pi_H \rightarrow \pi_L^*)$ ⇝ $T_1(\pi_H \rightarrow \pi_L^*)$ and {$S_2(\pi_{H-1} \rightarrow \pi_L^*)$ ⇝ T_1,$T_2(\pi \rightarrow \pi^*)$} ISC channels have been estimated to be less efficient ($k_{ISC} \approx 10^5$–10^6 s^{-1}). Based on the computed ISC rate constants and excited-state solvent shifts, it is suggested that the efficient triplet quantum yield of thionine in water is primarily due to the $S_1(\pi_H \rightarrow \pi_L^*)$ ⇝ $T_2(\pi_{H-1} \rightarrow \pi_L^*)$ channel with a computed rate constant of the order of 10^8–10^9 s^{-1} which is in accord with the experimental finding ($k_{ISC} = 2.8 \times 10^9$ s^{-1}).

1. Introduction

Thionine (3,7-diamino-phenothiazin-5-ium, Fig. 1) is the smallest member of the cationic phenothiazinum family of dyes. These photosensitizers have been used for a variety of applications including energy conversion[1,2] and photodynamic therapy.[3,4] It has been recognized that the photodynamic action of thionine and its derivatives in the presence of oxygen proceeds efficiently by either involving direct excited-state reactions such as electron transfer and hydrogen abstraction,[5,6] or by the formation of singlet oxygen.[7] Both mechanisms proceed *via* the triplet state of the dye. However, it is still not clear how intersystem crossing (ISC) leads to an efficient population of the triplet state.

In our previous work[8] we have examined the molecular and electronic structure of thionine in a vacuum and an aqueous environment (TH^+3Wa and TH^+5W) on the basis of quantum chemical calculations. We explored the potential energy surfaces

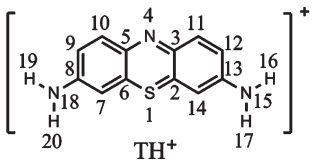

Fig. 1 Chemical structure and atom labeling for thionine.

and the relevant low-lying excited states that could participate in the photophysics of thionine using a combination of (time-dependent) density functional theory ((TD-)DFT)[9] and a DFT/multi-reference configuration interaction (DFT/MRCI)[10] method. The lowest singlet and triplet states were found to be of $\pi \rightarrow \pi^*$ (S_1, S_2, T_1 and T_2) and $n \rightarrow \pi^*$ (S_3 and T_3) character, S_1 being the spectroscopically bright state. The calculated vertical excitation energy of the S_1 state in water is 572 nm using the TH^+3Wa solvation model which agrees quite well with the reported experimental absorption maximum at 597 nm in diluted aqueous solutions.[11]

After photoexcitation of thionine, the first singlet excited state S_1 is populated and can either decay *via* fluorescence, non-radiatively (internal conversion) to the electronic ground state, or undergo a singlet–triplet ISC ($\phi_T = 0.55$).[12] Thionine fluoresces with an emission maximum at 610–625 nm[13,14] and it has been found that its quantum yield changes with solvent and concentration (*e.g.* $\varphi_F \approx 0.20$ in ethanol and $\phi_F \approx 0.1$–0.027 with increasing concentration of thionine in aqueous solutions).[15–17] A theoretical value of 602 nm has been obtained for this transition,[8] taking into account the vertical emission energy at the S_1 minimum and applying the solvent shift from the TH^+3Wa

[a]*Grupo de Bioquímica Teórica, Universidad Industrial de Santander, Carrera 27, Calle 9, Bucaramanga, Colombia. E-mail: mcdaza@uis.edu.co; Fax: +57 763 23778; Tel: +57 763 23778*
[b]*Institute of Theoretical and Computational Chemistry, Heinrich Heine University of Düsseldorf, Universitätsstr. 1, D-40225 Düsseldorf, Germany. E-mail: Christel.Marian@uni-duesseldorf.de; Fax: +49 (0)211 8113466; Tel: +49 (0)211 8113209*
[c]*Facultad de Química Ambiental, Universidad Santo Tomás, Carrera 18 No. 9-27, Bucaramanga, Colombia. E-mail: markusdoerr@gmx.de; Fax: +57 76712677; Tel: +57 76800801*

†Electronic supplementary information (ESI) available: Collection of results with regard to the sensitivity of the calculated ISC rate constants to different technical parameters. See DOI: 10.1039/c2pp25224d

model. Henceforth, this solvation model is employed for further discussions. From time-resolved experiments in diluted aqueous solutions, the singlet state lifetime of 360 ps and a fluorescence rate of 1.31×10^8 s^{-1} have been determined.[18] Furthermore, it has been suggested that the $S_1 \rightsquigarrow T_1$ ISC in photoexcited thionine may occur efficiently at a rate of $k_{ISC} = 2.8 \times 10^9$ s^{-1} in aqueous solutions.[19]

In order to gain further insight into the production of triplet thionine, we present a systematic investigation of the ISC mechanisms that could determine the efficiency of the concurrent decay processes. After photoexcitation to the S_1 bright state, its efficient non-radiative decay *via* ISC will depend on the energetic difference and the strength of the spin–orbit coupling (SOC) to the target triplet state, as well as the density of vibrational levels in the accepting state.

According to Lower and El-Sayed,[20] ISC is very efficient if the radiationless transition involves a change of orbital type. SOC between $\pi \rightarrow \pi^*$ and $n \rightarrow \pi^*$ states is in general much larger than between two $\pi \rightarrow \pi^*$ states. Thus, in the framework of the Condon approximation (direct SOC), the ISC rate constants for $(\pi \rightarrow \pi^*) \rightsquigarrow (n \rightarrow \pi^*)$ processes will be in general larger than for $(\pi \rightarrow \pi^*) \rightsquigarrow (\pi \rightarrow \pi^*)$. The computed $T_3(n \rightarrow \pi_L^*)$ adiabatic minimum lies about 0.02 eV above the $S_1(\pi_H \rightarrow \pi_L^*)$ minimum in the gas phase.[8] The energetic accessibility of $T_3(n \rightarrow \pi_L^*)$ from $S_1(\pi_H \rightarrow \pi_L^*)$ is somewhat uncertain taking into account the error bars of the method. This channel, however, is completely non-feasible in water, where the $T_3(n \rightarrow \pi_L^*)$ state is strongly blueshifted. Therefore, the $S_1(\pi_H \rightarrow \pi_L^*) \rightsquigarrow T_3(n \rightarrow \pi_L^*)$ ISC channel does not explain the efficient ISC of thionine in water.

As recent studies have shown, vibronic SOC could enhance the ISC constants between two $\pi \rightarrow \pi^*$ states taking into account a Herzberg–Teller type expansion of the SOC.[21–23] The two low-lying triplet excited states T_1 and $T_2(\pi \rightarrow \pi^*)$ lie energetically below the $S_1(\pi_H \rightarrow \pi_L^*)$ state. They could be considered as target states for efficient ISC in thionine. Hence, the present computational study is focused on the $\{S_1(\pi_H \rightarrow \pi_L^*) \rightsquigarrow T_1,T_2\text{-}(\pi \rightarrow \pi^*)\}$ ISC driven by vibronic SOC which can allow for an efficient population of the T_1 state. The radiative and non-radiative rate constants have been computed in a vacuum and their implications on the photophysics in aqueous solutions are discussed.

2. Methods and computational details

The equilibrium geometries of the electronic ground and excited states of thionine are taken from our previous work.[8] These structures were obtained at the level of density functional theory (DFT) or time-dependent density functional theory (TDDFT)[9] using the B3LYP[24,25] functional and TZVP[26] basis set as implemented in the Turbomole 6.3[27] program package. The Cartesian coordinate system was chosen in a way that the *xz* plane coincides with the molecular plane and the $C_2(y)$ axis passes through the phenothiazinium central ring. Harmonic vibrational frequencies were computed numerically employing the SNF program.[28] The vertical and adiabatic excitation energies, dipole moments and oscillator strengths at the computed minima were already presented in ref. 8 and were obtained from the DFT/MRCI[10] method. In order to understand the possible deactivation channels in aqueous solutions, estimates of the adiabatic excitation energies in water have been calculated by applying the spectroscopic shifts obtained with our best model (TH^+3Wa) to the adiabatic excitation energies in a vacuum. In this model, the vertical excitation energies of thionine in water were calculated introducing the spectral shifts due to electrostatic interaction employing the conductor-like screening model (COSMO, dielectric constant: $\varepsilon = 78$) and three explicit water molecules to simulate the effects of hydrogen bonding.[8]

Rate constants for ISC (k_{ISC}) from the S_1 and $S_2(\pi \rightarrow \pi^*)$ states to the *x*, *y* and *z* components of the first two low-lying triplet states (T_1 and $T_2(\pi \rightarrow \pi^*)$) were calculated using the VIBES program.[29] In this framework, the ISC constants were evaluated using a discretized form of the Fermi Golden Rule expression, (1):[30,31]

$$k_{ISC}(i \rightarrow f) = \frac{2\pi}{\hbar\eta} \sum_{|E_{f,\nu'} - E_{i,\nu=0}| < \eta} |H^{SO}_{\nu=0,\nu'}|^2 \qquad (1)$$

where the vectors ν and ν' represent the sets of vibrational quantum numbers in all normal modes of the initial $|i,\nu\rangle$ and final $|f,\nu'\rangle$ states, and $H^{SO}_{\nu=0,\nu'}$ represents the SOMEs driving the radiationless transition. Only those levels of the final state contribute which lie in a chosen interval of width 2η centered around the energy $E_{i,\nu=0}$ of the initial state. That means, instead of treating a strictly isoenergetic transition, an interval of final states is considered taking into account all final states within $\pm\eta$ of the vibronic energy of the initial level. Consequently, the results depend on the choice of η: it should be as small as possible because the transition $i \rightarrow f$ should be isoenergetic but large enough to cover a sufficient number of acceptor states. The effect of different choices for the interval width parameter η ranging from 0.001 to 100 cm^{-1} on the calculated ISC rates is presented in the ESI.†

In order to obtain the coupling matrix elements in eqn (1), $H^{SO}_{\nu=0,\nu'}$was expanded in a Taylor expansion in the normal coordinates $\{q_k\}$ around the minimum of the $S_1(\pi_H \rightarrow \pi_L^*)$ state as a reference point $\boldsymbol{q}_0$, (2):

$$H^{SO}_{\nu=0,\nu'} = \underbrace{\langle i|\hat{H}_{SO}|f\rangle|_{\boldsymbol{q}_0=0}\langle \nu = 0|\nu'\rangle}_{FC} + \underbrace{\sum_k \left(\frac{\partial}{\partial q_k}\langle i|\hat{H}_{SO}|f\rangle\right)\Big|_{\boldsymbol{q}_0=0} \langle \nu = 0|q_k|\nu'\rangle + O\left(|\boldsymbol{q}|^2\right)}_{HT} \qquad (2)$$

The first term labeled FC in eqn (2) is the so-called Condon approximation which neglects the dependence of the coupling matrix element on the molecular structure. The purely electronic matrix element $\lceil i|\hat{H}_{SO}|f\rangle$ is denominated direct SOC in the following. The expansion in eqn (2) closely resembles the usual Herzberg–Teller (HT) treatment of the electronic dipole transition matrix elements. Thus, this first-order derivative coupling is named vibronic SOC. The computation of the $\{S_1, S_2\ (\pi \rightarrow \pi^*) \rightsquigarrow T_1, T_2(\pi \rightarrow \pi^*)\}$ ISC rate constants was performed taking vibronic SOC into account.

For the computation of the SOMEs $\langle i|\hat{H}_{SO}|f\rangle$ between the correlated DFT/MRCI wavefunctions, we used the spin–orbit coupling kit SPOCK[32–34] where the one-center mean-field approximation[35] to the Breit–Pauli Hamiltonian is used for the description of the SOC. To evaluate the HT term in eqn (2), the first-order derivatives of the SOMEs with respect to the normal mode coordinates were calculated numerically by finite difference techniques by means of the symmetrized two-point formula (3):

$$\frac{\partial}{\partial q_k}\langle i|\hat{H}_{SO}|f\rangle \approx \frac{\langle i|\hat{H}_{SO}|f\rangle\big|_{\boldsymbol{q}_0+\varepsilon\mathbf{e}_k} - \langle i|\hat{H}_{SO}|f\rangle\big|_{\boldsymbol{q}_0-\varepsilon\mathbf{e}_k}}{2\varepsilon} \quad (3)$$

where $\mathbf{e}_k$ denotes the unit vector pointing into the direction of the normal mode q_k and ε represents the displacement increment referring to dimensionless harmonic oscillator coordinates q_k (set to ε = 0.1). Single-point DFT/MRCI and SOMEs calculations have been carried out at the two distorted geometries $\boldsymbol{q}_0 \pm \varepsilon\mathbf{e}_k$ for each normal mode. The CI space from a preceding DFT/MRCI run without symmetry constraints at the reference geometry $\boldsymbol{q}_0$ was used while the molecular orbitals were reoptimized in all calculations. Furthermore, the phases of the SOMEs of the $S_1(\pi_H \rightarrow \pi_L^*)/T_1(\pi_H \rightarrow \pi_L^*)$ and $S_1(\pi_H \rightarrow \pi_L^*)/T_2(\pi_{H-1} \rightarrow \pi_L^*)$ couplings at each distorted geometry of the $S_1(\pi_H \rightarrow \pi_L^*)$ minimum were obtained by relating their phases to the sign of the $S_1(\pi_H \rightarrow \pi_L^*)/T_3(n \rightarrow \pi_L^*)$ and $T_2(\pi_{H-1} \rightarrow \pi_L^*)/T_3(n \rightarrow \pi_L^*)$ SOMEs as reference for the calculation of the sign of the derivatives. For more details see ref. 21.

In thionine there are a total of 72 vibrational modes. When vibronic SOC is taken into account, typically, the derivatives of the SOMEs along *out-of-plane* vibrational modes become important and the totally symmetric modes act as possible accepting modes. Taking into account the choice of the mirror plane as the *xz*-plane of the C_{2v} molecular point group in this work and symmetry arguments, we included the vibronic SOC terms arising from the eleven A_2 and twelve B_2 *out-of-plane* promoting modes in the calculation of the ISC rate constants of the $S_1{}^1B_1(\pi_H \rightarrow \pi_L^*) \rightsquigarrow T_1{}^3B_1(\pi_H \rightarrow \pi_L^*)$ and $S_1{}^1B_1(\pi_H \rightarrow \pi_L^*) \rightsquigarrow T_2{}^3A_1(\pi_{H-1} \rightarrow \pi_L^*)$ channels. Our first calculations including only the 25 symmetric A_1 modes as accepting modes lead to very low ISC rate constants. Therefore we tested the influence of the asymmetric modes using all 49 *in-plane* modes as accepting modes in the calculation. Moreover, test calculations including the 72 *out-of-plane* and *in-plane* modes as accepting modes were performed.

In order to get more information about the coupling between states, a linearly-interpolated path between the $S_1{}^1B_1(\pi_H \rightarrow \pi_L^*)$ and $T_2{}^3A_1(\pi_H \rightarrow \pi_L^*)$ minima was constructed using the program DISTORT.[29] At each of the 20 grid points, a single-point DFT/MRCI calculation was carried out to determine the vertical excitation energies of the singlet and triplet manifolds.

In addition to the triplet quantum yield, a further essential parameter for the singlet oxygen generation capability of a photosensitizer is the lifetime of its T_1 state. Possible intramolecular decay channels are the nonradiative (ISC) and radiative (phosphorescence) relaxation to the electronic ground state. To obtain an estimate of the corresponding rate constants, SOMEs have been evaluated at the T_1 minimum geometry. Spin–orbit mixed wavefunctions for the calculation of phosphorescence rates have been computed at the multi-reference spin–orbit configuration interaction (MRSOCI) level, since sum-over-states perturbation theory expansions of phosphorescence rates have been shown to converge very slowly with the number of intermediate electronic states.[35] Due to the small spin–orbit splitting of the T_1 sublevels, the convergence threshold of the Davidson iterative procedure in the MRSOCI step was set to 5×10^{-9} E_h. Using transition dipole moments ($\mu_{el}(S_0 \leftarrow T_{1,\zeta})$) of the spin–orbit mixed MRSOCI wavefunctions in atomic units and the energy difference between the T_1 and S_0 states in reciprocal centimeters ($\Delta E_{S_0 \leftarrow T_{1,\zeta}}$), the phosphorescence rate is ($\Gamma_{1,\zeta}$) obtained according to eqn (4):

$$\Gamma_{1,\zeta} = \frac{4e^2}{3c^3\hbar^4}\Delta E^3_{S_0 \leftarrow T_{1,\zeta}}\left|\mu_{el}\left(S_0 \leftarrow T_{1,\zeta}\right)\right|^2 \quad (4)$$

3. Results and discussion

3.1. Vertical and adiabatic excitation energies: energetically accessible intersystem crossing channels

A detailed discussion of the computed gas phase and solvated vertical electronic spectrum as well as the optimized excited state geometries and adiabatic energies is given in our previous work.[8] Here, we provide a short summary of important features for the discussion of the available ISC channels. An overview of the DFT/MRCI adiabatic excitation energies is given in Table 1 and the shapes of the relevant molecular frontier orbitals are depicted in Fig. 2.

At the calculated C_{2v}-symmetric ground state, the vertical excitation spectrum predicts the two lowest singlet and triplet states to be of $\pi \rightarrow \pi^*$ character. The $S_1(\pi_H \rightarrow \pi_L^*)$ state which is the spectroscopically bright state has a vertical excitation energy of 2.29 eV. The optically dark $S_2(\pi_{H-1} \rightarrow \pi_L^*)$ state is vertically located 0.20 eV higher in energy than the $S_1(\pi_H \rightarrow \pi_L^*)$ state. In the triplet manifold, the $T_1(\pi_H \rightarrow \pi_L^*)$ and $T_2(\pi_{H-1} \rightarrow \pi_L^*)$ states are energetically below the $S_1(\pi_H \rightarrow \pi_L^*)$ state (by 0.66 and 0.18 eV, respectively). Above S_2 and S_1 is the $T_3(n \rightarrow \pi_L^*)$ state at 2.78 eV.

The $S_1(\pi_H \rightarrow \pi_L^*)$ state shows an adiabatic excitation energy of 2.27 eV. The estimated fluorescence rate from $S_1(\pi_H \rightarrow \pi_L^*)$

Table 1 Adiabatic singlet and triplet DFT/MRCI excitation energies ΔE^{ad} (eV) of the excited states of TH^+ computed using the TZVP basis set. Oscillator strengths for emission at the excited-state minima are listed in parentheses

Geometry	Electronic structure[a]	Vacuum[b]	Aqueous solution[c]
$S_1(C_{2v}, 1^1B_1)$	(0.80) $\pi_H \rightarrow \pi_L^*$	2.27(0.790)	2.14
$S_2(C_s, 2^1A')$	(0.45) $\pi_{H-1} \rightarrow \pi_L^*$(0.36) $\pi_H \rightarrow \pi_L^*$	2.29(0.269)	2.23
$T_1(C_{2v}, 1^3B_1)$	(0.92) $\pi_H \rightarrow \pi_L^*$	1.63	1.46
$T_2(C_{2v}, 1^3A_1)$	(0.88) $\pi_{H-1} \rightarrow \pi_L^*$	1.97	1.93
$T_3(C_1, 2^3A)$	(0.50) $n_{H-2} \rightarrow \pi_L^*$(0.26) $\pi_{H-4} \rightarrow \pi_L^*$	2.31	2.75

[a] Dominant contributions at the DFT/MRCI/TZVP level, ref. 8. [b] ΔE^{ad} from ref. 8. [c] Estimates for ΔE^{ad} in aqueous solution calculated applying the vertical excitation energy shifts of the TH^+3Wa model from ref. 8.

is low ($k_F \approx 1.66 \times 10^8$ s^{-1}) and in excellent agreement with the experimental value in water.[18] Taking the applicability of Kasha's rule for granted, the bright $S_1(\pi_H \rightarrow \pi_L^*)$ state should be the only eligible ISC promoting state and a large population of this state is expected when the molecule is photoexcited. However, the minima of the $S_2(\pi_{H-1} \rightarrow \pi_L^*)$ and $S_1(\pi_H \rightarrow \pi_L^*)$ states are almost degenerate. In fact, a conical intersection has been already found along a linearly interpolated path connecting these two minima. Due to their energetic proximity and the mixing between the $(\pi_H \rightarrow \pi_L^*)$ and $(\pi_{H-1} \rightarrow \pi_L^*)$ transitions at the S_2 minimum, a small population of this state might be expected (noted by the increase of the oscillator strength, see Table 1) and ISC channels from this state may also be energetically plausible.

The C_{2v} symmetric $T_1(\pi_H \rightarrow \pi_L^*)$ and $T_2(\pi_{H-1} \rightarrow \pi_L^*)$ minima show up adiabatically below the $S_1(\pi_H \rightarrow \pi_L^*)$ minimum, at 1.63 and 1.97 eV, respectively. The $T_3(n \rightarrow \pi_L^*)$ V-shaped minimum is located slightly above the S_1 and $S_2(\pi \rightarrow \pi^*)$ states (0.04 and 0.02 eV, respectively) and could be considered as quasi degenerate keeping in mind the uncertainties of the method in the calculated excitation energies (≈ 0.2 eV). In this framework, ISC to the $T_3(n \rightarrow \pi_L^*)$ without thermal activation might be plausible in the gas phase. However, it was found that the zero-point vibrational energy of the $T_3(n \rightarrow \pi_L^*)$ state is higher than that of the S_1 and $S_2(\pi \rightarrow \pi^*)$ states by about 0.2 eV. Furthermore, the $T_3(n \rightarrow \pi_L^*)$ state was found to experience a substantial blueshift relative to the $(\pi \rightarrow \pi^*)$ states in aqueous solutions making these channels inaccessible from the ground vibrational levels of the S_1 and $S_2(\pi \rightarrow \pi^*)$ states.[8] Thus, on the basis of these results, the T_1 and $T_2(\pi \rightarrow \pi^*)$ states have been considered as main target states for effective ISC channels.

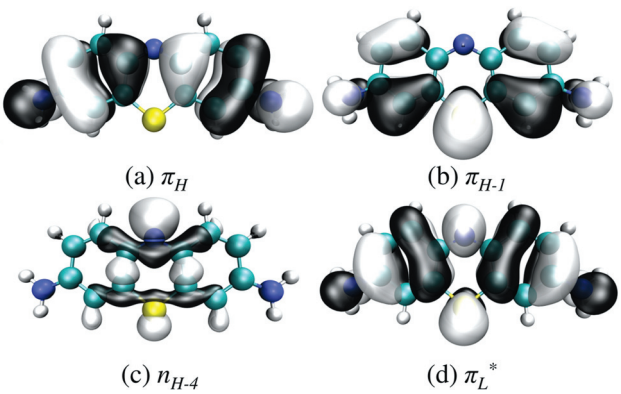

Fig. 2 Frontier BHLYP/TZVP Kohn–Sham molecular orbitals computed at the ground-state (S_0) minimum of TH^+ (isovalue 0.03).

3.1.1. Dependency of spin–orbit coupling on molecular structure. ISC rates do not only depend on the energy gap between the involved states but also on the strength of the SOC, which can be estimated quantitatively by the evaluation of the SOMEs. The computed purely electronic SOMEs $\lceil i|\hat{H}_{SO}|f\rangle$ at the S_1, S_2 and $T_1(\pi \rightarrow \pi^*)$ minima of thionine are compiled in Table 2. The results show that the magnitude of the SOMEs does not change when going from the S_1 to the $T_1(\pi \rightarrow \pi^*)$ minimum. This is an indication that the SOMEs are relatively insensitive to *in-plane* motions at these minima. According to symmetry selection rules, the $\lceil {}^1A_1|\hat{H}_{SO}|{}^3A_1\rangle$ and $\lceil {}^1B_1|\hat{H}_{SO}|{}^3B_1\rangle$ $(\pi \rightarrow \pi^*)$ transitions are forbidden and hence all the corresponding SOMEs vanish at these C_{2v}-symmetric minima.

At the $S_1(\pi_H \rightarrow \pi_L^*)$ minimum, small coupling matrix elements (≈ 0.4 cm^{-1}) between the $S_1(\pi_H \rightarrow \pi_L^*)$ and $T_3(n \rightarrow \pi_L^*)$ states are found. Following the El-Sayed rules, these small values of the SOMEs are rather unexpected due to the character of the states involved in the transition. Instead, it is found that the coupling at the $S_2(\pi_{H-1} \rightarrow \pi_L^*)/T_3(n \rightarrow \pi_L^*)$ pair is two orders of magnitude larger, up to 9.90 cm^{-1}. These larger SOMEs could be explained due to a heavy-atom effect, in this case the higher probability for the electrons to be at the sulphur center in the molecular orbitals π_{H-1} and n_{H-4} involved in the coupling. In contrast, no electron density is found at the sulphur center in the π_H orbital that is decisive for the $S_1(\pi_H \rightarrow \pi_L^*)/T_3(n \rightarrow \pi_L^*)$ interaction (see Fig. 2).

The coupling between the states follows somewhat different trends at the $S_2(\pi_{H-1} \rightarrow \pi_L^*)$ minimum. The interactions of the $S_1(\pi_H \rightarrow \pi_L^*)$ and $S_2(\pi_{H-1} \rightarrow \pi_L^*)$ states with the $T_3(n \rightarrow \pi_L^*)$ state are nearly of the same magnitude in their x and y components at this geometry. At this point, the $S_1(\pi_H \rightarrow \pi_L^*)$ state is composed of an additional contribution of the $\pi_{H-1} \rightarrow \pi_L^*$ transition (nearly 50%).[8] Therefore, the S_1/T_3 coupling significantly increases as a consequence of the larger coupling between the $n \rightarrow \pi_L^*$ with the $\pi_{H-1} \rightarrow \pi_L^*$ configurations. As expected, the opposite trend could be found for the coupling between the S_2 and T_3 states.

As noted before, the SOC between the S_1, S_2 and the T_1 and $T_2(\pi \rightarrow \pi^*)$ states is either small or symmetry forbidden. Nevertheless, the population of *out-of-plane* vibrational states can lead to an increase of these couplings. The dependence of the $\lceil S_1|$

Table 2 Spin–orbit matrix elements $\lceil i|\hat{H}_{SO}|f\rangle$ (SOMEs, cm^{-1}) between low-lying singlet and triplet states at the $S_1(\pi_H \rightarrow \pi_L^*)$, $S_2(\pi_{H-1} \rightarrow \pi_L^*)$ and $T_1(\pi_H \rightarrow \pi_L^*)$ equilibrium geometries. [a] The direction of the coupling x, y or z is given in parenthesis

SOMEs $\lceil i\|\hat{H}_{SO}\|f\rangle$	@$S_1(\pi_H \rightarrow \pi_L^*)$	@$S_2(\pi_{H-1} \rightarrow \pi_L^*)$	@$T_1(\pi_H \rightarrow \pi_L^*)$
$\lceil S_0\|\hat{H}_{SO}\|T_1(\pi_H \rightarrow \pi_L^*)\rangle$	0.01(y)	0.02(y)	0.00(y)
$\lceil S_1(\pi_H \rightarrow \pi_L^*)\|\hat{H}_{SO}\|T_1(\pi_H \rightarrow \pi_L^*)\rangle$	—	0.02(z)	—
$\lceil S_1(\pi_H \rightarrow \pi_L^*)\|\hat{H}_{SO}\|T_2(\pi_{H-1} \rightarrow \pi_L^*)\rangle$	−0.08(y)	0.06(z)	−0.09(y)
$\lceil S_1(\pi_H \rightarrow \pi_L^*)\|\hat{H}_{SO}\|T_3(n \rightarrow \pi_L^*)\rangle$	0.39(z)	5.92(x)/−1.09(y)	−0.42(z)
$\lceil S_2(\pi_{H-1} \rightarrow \pi_L^*)\|\hat{H}_{SO}\|T_1(\pi_H \rightarrow \pi_L^*)\rangle$	−0.02(y)	−0.02(z)	−0.02(y)
$\lceil S_2(\pi_{H-1} \rightarrow \pi_L^*)\|\hat{H}_{SO}\|T_2(\pi_{H-1} \rightarrow \pi_L^*)\rangle$	—	0.05(z)	—
$\lceil S_2(\pi_{H-1} \rightarrow \pi_L^*)\|\hat{H}_{SO}\|T_3(n \rightarrow \pi_L^*)\rangle$	−9.90(x)	−6.88(x)/0.89(y)	10.55(x)

[a] The $S_1(\pi_H \rightarrow \pi_L^*)$, $T_1(\pi_H \rightarrow \pi_L^*)$ and $T_2(\pi_{H-1} \rightarrow \pi_L^*)$ minima are C_{2v} symmetric and the $S_2(\pi_{H-1} \rightarrow \pi_L^*)$ minimum is C_s symmetric.

$\hat{H}_{SO}|T_{\{1x,1z,2x,2z\}}\rangle$ SOMEs on displacements along selected A_2 and the B_2 *out-of-plane* vibrational coordinates at the $S_1(\pi_H \rightarrow \pi_L^*)$ minimum is depicted in Fig. 3. In addition, the vibrational normal modes and the numerical derivatives of these SOMEs are presented in Fig. 4 and Table 3, respectively. Once the system is distorted along these *out-of-plane* modes, the point group selection rules do not hold and the SOMEs of these $\pi \rightarrow \pi^*$ states could increase to an extent which depends on how the distorted geometry can allow an efficient interaction with the $n \rightarrow \pi^*$ state. The most important increase in magnitude is obtained for the SOMEs $\lceil S_1|\hat{H}_{SO}|T_{2(x,z)}\rangle$ upon the geometry distortions along the ν_1 and ν_8 normal mode coordinates. The lowest vibrational coupling mode ν_1 is of A_2 symmetry, exhibits a frequency of 50.0 cm^{-1} which corresponds to an asymmetric deformation of the phenothiazinium ring and promotes an increase of the $\lceil S_1|\hat{H}_{SO}|T_{2x}\rangle$ SOME up to ≈3.2 cm^{-1} for a displacement by two unit lengths. The symmetric (B_2) ν_8 mode shows up at 263.7 $cm^{-1}$and leads to an increase of the $\lceil S_1|\hat{H}_{SO}|T_{2z}\rangle$ matrix element (≈ 4.0 cm^{-1}, see Fig. 3). This mode corresponds to a

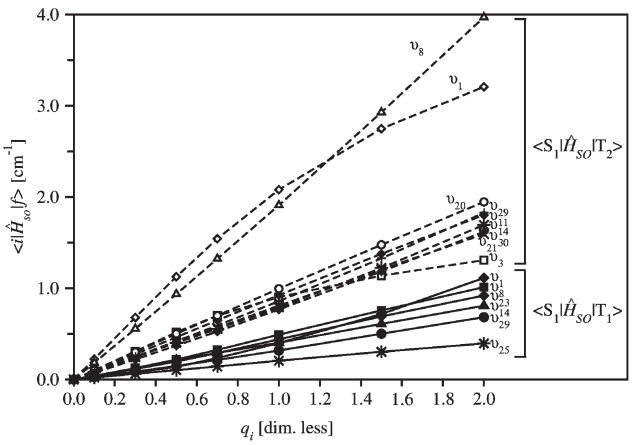

Fig. 3 Change of the SOMEs upon elongation of the *out-of-plane* vibrational normal modes. The SOMEs $\lceil S_1|\hat{H}_{SO}|T_1\rangle$ are represented by solid lines and the SOMEs $\lceil S_1|\hat{H}_{SO}|T_2\rangle$ by dashed lines.

Table 3 Harmonic frequencies $\bar{\nu}_i$ (cm^{-1}) of the *out-of-plane* modes and derivatives of the SOMEs with respect to the corresponding dimensionless normal coordinates at the $S_1(\pi_H \rightarrow \pi_L^*)$ minimum. The direction of the coupling x or z is given in parentheses

Mode number	$\bar{\nu}_i$	$\frac{\partial\langle S_1\|\hat{H}_{SO}\|T_1\rangle}{\partial q_i}$	$\frac{\partial\langle S_1\|\hat{H}_{SO}\|T_2\rangle}{\partial q_i}$
$\nu_1(A_2)$	50.0	−0.27(z)	−2.23(x)
$\nu_3(A_2)$	127.2	−0.18(z)	−1.00(x)
$\nu_5(A_2)$	170.3	0.05(z)	0.12(x)
$\nu_{11}(A_2)$	304.2	0.14(z)	−0.93(x)
$\nu_{14}(A_2)$	404.9	−0.41(z)	0.84(x)
$\nu_{17}(A_2)$	477.2	0.01(z)	−0.14(x)
$\nu_{21}(A_2)$	534.0	0.14(z)	−0.81(x)
$\nu_{25}(A_2)$	586.6	0.21(z)	−0.41(x)
$\nu_{29}(A_2)$	781.4	0.28(z)	−0.83(x)
$\nu_{32}(A_2)$	826.4	0.05(z)	−0.44(x)
$\nu_{37}(A_2)$	947.7	−0.03(z)	0.41(x)
$\nu_2(B_2)$	56.2	0.06(x)	−0.11(z)
$\nu_4(B_2)$	169.2	0.19(x)	−0.19(z)
$\nu_7(B_2)$	178.5	0.00(x)	0.37(z)
$\nu_8(B_2)$	263.7	0.39(x)	−1.84(z)
$\nu_{13}(B_2)$	397.9	−0.06(x)	−0.33(z)
$\nu_{18}(B_2)$	477.9	−0.02(x)	−0.09(z)
$\nu_{20}(B_2)$	527.0	−0.08(x)	1.00(z)
$\nu_{23}(B_2)$	563.7	0.38(x)	−0.53(z)
$\nu_{24}(B_2)$	581.8	−0.06(x)	0.64(z)
$\nu_{30}(B_2)$	788.5	−0.19(x)	0.73(z)
$\nu_{33}(B_2)$	830.1	−0.09(x)	0.32(z)
$\nu_{38}(B_2)$	950.1	−0.06(x)	0.12(z)

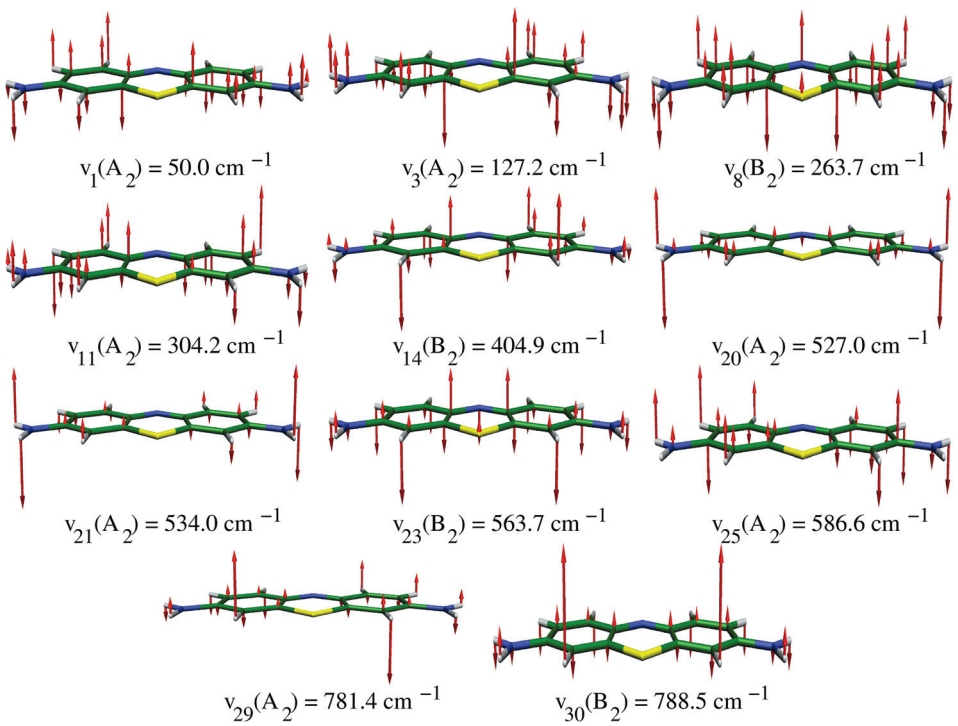

Fig. 4 Important coupling vibrational normal modes at the $S_1(\pi_H \rightarrow \pi_L^*)$ minimum of thionine.

Table 4 Calculated rate constants k_{ISC} (s^{-1}) in a vacuum for the $S_i \rightarrow T_{i(x,z)}$ (i = 1,2) channels. Other columns: adiabatic energy difference (ΔE^{ad}, eV), number of derivatives with respect to *out-of-plane* modes ($\#_{derivs}$), number of accepting modes ($\#_{acc}$), width of the search interval η (cm^{-1}) and number of final state vibrational levels within the search interval ($\#_{\nu'}$)

Channel	ΔE^{ad}	$\#_{derivs}$	$\#_{acc}$	η	$\#_{\nu'}$	k_{ISC}
$S_1 \rightarrow T_{1x}$	0.64	12	25	0.1	6×10^4	2.73×10^3
$S_1 \rightarrow T_{1x}$	0.64	12	49	0.1	3×10^6	2.40×10^5
$S_1 \rightarrow T_{1x}$	0.68[a]	12	49	0.1	7×10^6	3.06×10^5
$S_1 \rightarrow T_{1z}$	0.64	11	25	0.1	4×10^4	3.62×10^3
$S_1 \rightarrow T_{1z}$	0.64	11	49	0.1	2×10^6	2.14×10^5
$S_1 \rightarrow T_{1z}$	0.68[a]	11	49	0.1	5×10^6	1.27×10^6
$S_1 \rightarrow T_{2x}$	0.30	11	49	0.1	5×10^3	1.55×10^8
$S_1 \rightarrow T_{2x}$	0.30	1[b]	49	0.1	5×10^3	1.28×10^8
$S_1 \rightarrow T_{2x}$	0.21[a]	11	49	0.1	7×10^2	1.29×10^9
$S_1 \rightarrow T_{2z}$	0.30	12	25	0.1	4×10^2	1.93×10^7
$S_1 \rightarrow T_{2z}$	0.30	12	49	0.1	4×10^3	6.30×10^7
$S_1 \rightarrow T_{2z}$	0.30	12	72	0.1	1×10^5	1.39×10^8
$S_1 \rightarrow T_{2z}$	0.30	1[c]	49	0.1	4×10^3	1.48×10^7
$S_1 \rightarrow T_{2z}$	0.21[a]	12	49	0.1	6×10^2	3.72×10^6

Rate constants calculated: applying spectroscopic solvation shifts from models [a] TH^+3Wa, ref. 8; including only the [b] mode ν_1 and [c] mode ν_8 cm^{-1}.

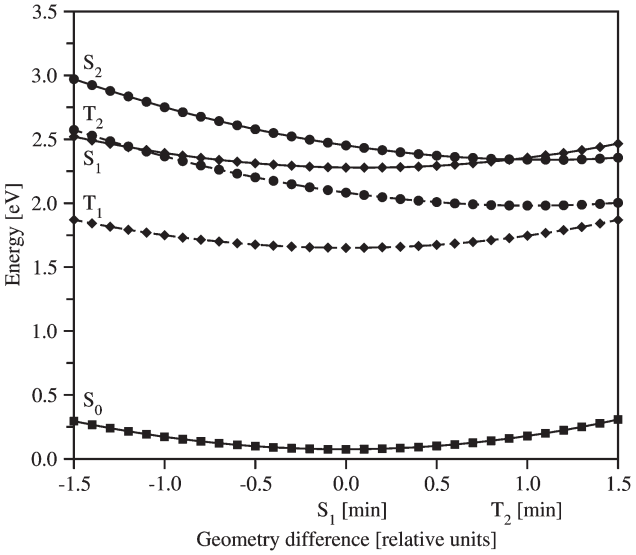

Fig. 5 Thionine DFT/MRCI energies of the low-lying states along a linearly interpolated path between the $S_1(\pi_H \rightarrow \pi_L^*)$ and $T_2(\pi_{H-1} \rightarrow \pi_L^*)$ minima. The singlet profiles are represented by solid lines and the triplet profiles by dashed lines.

symmetric deformation of the phenothiazinium which includes a pyramidalization of the nitrogen and sulphur atoms of the central ring. Noteworthy, ν_1 and ν_8 should be considered here as important promoting modes for the $S_1(\pi_H \rightarrow \pi_L^*) \rightsquigarrow T_2(\pi_{H-1} \rightarrow \pi_L^*)$ decay channel since they are able to induce an efficient mixing between n and π molecular orbitals. In contrast, only modest increments of the $\lceil S_1|\hat{H}_{SO}|T_{1x/z}\rangle$ SOMEs are found along these normal modes (≈ 1 cm^{-1}, see Fig. 3). This appears reasonable taking into account that these states possess the same $\pi_H \rightarrow \pi_L^*$ character which is not able to induce efficient coupling with the $n \rightarrow \pi_L^*$ transition.

The increase of the SOMEs along the vibrational mode coordinates shown in Fig. 3 is seen to be mostly linear. Only a few deviations from the linearity are noticeable, in particular for the $\lceil S_1|\hat{H}_{SO}|T_{2x}\rangle$ coupling along the ν_1 and ν_3 A_2 normal modes. This has consequences for the magnitude of the calculated derivatives of the SOMEs for the coupling of the S_1 and $T_2(\pi \rightarrow \pi^*)$ states in the x and z components: the derivative along the ν_1 A_2 mode (2.23 cm^{-1}) is larger than that obtained at the ν_8 mode (1.84 cm^{-1}) in opposition to the trend observed in Fig. 3. In addition, substantial contributions to the $S_1/T_2(\pi \rightarrow \pi^*)$ vibronic SOC originating from ν_3, ν_{11}, ν_{14}, ν_{20}, ν_{21}, and ν_{30} normal modes are obtained.

3.1.2. Intersystem crossing channels in a vacuum. The results of the $\{S_1(\pi \rightarrow \pi^*) \rightsquigarrow T_1,T_2(\pi \rightarrow \pi^*)\}$ ISC rate constants obtained from the golden rule evaluation and taking vibronic SOC into account are presented in Table 4, together with the parameters employed for the calculation of these rates. A more detailed overview about the technical parameters employed in the calculation of the ISC rate constants can be seen in the ESI.† Our results clearly show sizeable rate constants for the ISC from the zero vibrational level of the $S_1(\pi_H \rightarrow \pi_L^*)$ to the vibrational levels of the T_{2x} and $T_{2z}(\pi_{H-1} \rightarrow \pi_L^*)$ substates, being of the order of $\approx 10^8$ s^{-1}. In contrast, the ISC to the $T_1(\pi_H \rightarrow \pi_L^*)$ state is found to be much slower ($\approx 10^5$–10^6 s^{-1}). According to these results, the $S_1(\pi_H \rightarrow \pi_L^*) \rightsquigarrow T_2(\pi_{H-1} \rightarrow \pi_L^*)$ ISC is proposed as the main responsible channel for the efficient population of the triplet manifold. The participation of the ν_1 and ν_8 vibrational normal modes as important promoting modes can be quantitatively observed by accounting for the derivatives of these individual modes only in the calculation of the ISC rate (see Table 4). Their contributions to the rate constant are of the order of $\approx 10^8$ and $\approx 10^7$ s^{-1}, respectively. Moreover, this channel benefits from a crossing between the $S_1(\pi_H \rightarrow \pi_L^*)$ and $T_2(\pi_{H-1} \rightarrow \pi_L^*)$ potential energy surfaces along a linearly interpolated path connecting the corresponding minima (see Fig. 5), increasing the overlap between the vibrational wavefunctions of the $S_1(\pi_H \rightarrow \pi_L^*) \rightsquigarrow T_2(\pi_{H-1} \rightarrow \pi_L^*)$ channel.

It is worth mentioning that the magnitude of the rate constants depends on the number of vibrational levels and *in-plane* accepting modes that is accounted for in the calculation. For example, including only the 25 A_1 accepting modes in the rate computation results in $k_{ISC}(S_1 \rightsquigarrow T_1) \approx 10^3$ s^{-1}, whereas an extension of the accepting modes to include the B_1 *in-plane* modes enhances the rate by two orders of magnitude, *i.e.*, to $\approx 10^5$ s^{-1}. For the $S_1(\pi \rightarrow \pi^*) \rightsquigarrow T_2(\pi \rightarrow \pi^*)$ channel, an increase by a factor of three is obtained in this case. A further enhancement by a factor of two is observed when all 72 vibrational modes are accounted for. This behaviour could be explained due to combination of two asymmetric modes that result in a totally symmetric A_1 mode. Furthermore, test calculations showed that the calculated ISC rate constants are quite sensitive to the S_1–T_2 energy gap. Therefore, the calculated $k_{ISC}(S_1 \rightsquigarrow T_2)$ values can be considered only as rough estimates. Details regarding these calculations are presented as ESI.†

To gain further insight, the $\{S_2(\pi_{H-1} \rightarrow \pi_L^*) \rightsquigarrow T_1(\pi_H \rightarrow \pi_L^*), T_2(\pi_{H-1} \rightarrow \pi_L^*)\}$ channels have also been analysed. The rate constants characterizing these transitions are presented in ESI (Table S6†). As aforementioned, the dark $S_2(\pi_{H-1} \rightarrow \pi_L^*)$

state may possibly be populated after vertical excitation to the $S_1(\pi_H \rightarrow \pi_L^*)$ state (ΔE = 0.20 eV) *via* conical intersection and $S_1(\pi_H \rightarrow \pi_L^*)$–$S_2(\pi_{H-1} \rightarrow \pi_L^*)$ character mixing. However, with an ISC rate constant of the order of $\approx 10^6$ s^{-1}, these channels cannot compete with the relaxation channel involving the $S_1(\pi_H \rightarrow \pi_L^*)$ state.

3.2. Intersystem crossing channels in water

In the following we present a qualitative discussion of the various possible decay channels available to the chromophore in aqueous solutions. For this purpose an estimate of the adiabatic excitation energies is obtained by applying solvent shifts to the individual electronic states (Table 1). The employed solvent shifts correspond to our best model TH^+3Wa. As is expected, the $T_3(n \rightarrow \pi_L^*)$ adiabatic excitation energy is strongly blueshifted to 2.75 eV, resulting in an adiabatic energy difference of 0.61 eV to the optically bright state in an aqueous medium as compared to 0.04 eV in a vacuum. As a consequence, the participation of any ISC channel involving the $T_3(n \rightarrow \pi_L^*)$ state in the photophysics of thionine in water can safely be ruled out.

The adiabatic excitation energies of the two low-lying triplet and singlet ($\pi \rightarrow \pi^*$) states experience very small red shifts. The adiabatic energy separation of the S_1 and $T_1(\pi \rightarrow \pi^*)$ states ($\Delta E^{ad}(S_1 \rightarrow T_1)$ = 0.68) is quite similar to the one calculated in the gas phase. As a consequence, the calculated $S_1(\pi_H \rightarrow \pi_L^*) \rightsquigarrow T_1(\pi_H \rightarrow \pi_L^*)$ ISC rate constants in water are also very similar to those found in a vacuum ($k_{ISC}(S_1 \rightarrow T_1) \approx 10^5$–$10^6$ s^{-1}, see also Table S7 in ESI†).

In contrast, the $\Delta E^{ad}(S_1 \rightarrow T_2)$ gap is decreased from 0.30 eV in a vacuum to 0.21 eV in our water model. This accelerates the $S_1(\pi_H \rightarrow \pi_L^*) \rightsquigarrow T_{2x}(\pi_{H-1} \rightarrow \pi_L^*)$ transition while reducing the efficiency of the $S_1(\pi_H \rightarrow \pi_L^*) \rightsquigarrow T_{2z}(\pi_{H-1} \rightarrow \pi_L^*)$ channel by one order of magnitude. As the total rate is the sum over the contributions of all channels, all-in-all the ISC rate is enhanced due to solvation. With a sufficient number of vibrational states within the search interval (η = 0.1) and 49 coupling accepting modes involved, a rate of $k_{ISC} \approx 10^9$ s^{-1} is obtained which is in very good agreement with the experimental value of $k_{ISC} = 2.8 \times 10^9$ s^{-1} in aqueous solutions.[19] Moreover, these results show that the $S_1(\pi_H \rightarrow \pi_L^*) \rightsquigarrow T_2(\pi_{H-1} \rightarrow \pi_L^*)$ channel should be considered as the main efficient channel for population transfer into the triplet manifold (ϕ_T = 0.55).[12] It thus may efficiently quench the fluorescence of the $S_1(\pi_H \rightarrow \pi_L^*)$ state ($k_F \approx 1.31 \times 10^8$ s^{-1})[18] in aqueous solutions which is evidenced by its smaller experimental quantum yield ($\phi_F \approx$ 0.1–0.027).[15–17] It should be kept in mind that many factors affect the rate constant, *e.g.* the thermodynamics of the water molecules including the geometrical relaxation of the excited states and their participation in the SOC. However, within the limitations of the computational models used in this work, the qualitative picture obtained is in very good accord with the experimental data, validating the results thus obtained.

3.3. Phosphorescence

In addition to energy transfer to $^3O_2$ and photo-redox reactions, the decay of the triplet excited state of thionine could include radiative or non-radiative relaxation processes. The radiative depopulation of the $T_1(\pi_H \rightarrow \pi_L^*)$ state to the ground state could result in phosphorescence which, however, in the case of thionine has never been observed. In order to check the consistency of our calculations with these findings, we calculated the $T_1(\pi_H \rightarrow \pi_L^*) \rightarrow S_0$ phosphorescence rates ($\Gamma_{1,\zeta}$), which are presented in Table 5. Since the $T_{1,a}$, $T_{1,b}$ and $T_{1,c}$ sublevels are degenerate, it can be assumed that each level is equally populated (high temperature average). The computed MRSOCI electronic transition dipole moments are all nearly zero, leading to very slow phosphorescence (from zero to 10^{-1} s^{-1}), which is common for radiative decay originating from "pure" $\pi \rightarrow \pi^*$ states.[36] The phosphorescence lifetime ($\tau_{P,\zeta}$) calculated from the averaged transition rate constants is very large ($\approx$ 4500 s) verifying the experimentally non-observed phosphorescence.

Table 5 Vertical excitation energies ($\Delta E_{S_0 \leftarrow T_{1,\zeta}}$, cm^{-1}), transition dipole moments ($\mu_{el}(S_0 \leftarrow T_{1,\zeta})$, a.u.), phosphorescence rates ($\Gamma_{1,\zeta}$, s^{-1}) and radiative lifetimes ($\tau_{P,\zeta}$, s) for the three fine-structure sublevels of the $T_1(\pi_H \rightarrow \pi_L^*)$ state. The polarization direction of $\mu_{el}(S_0 \leftarrow T_{1,\zeta})$ is given in parentheses

Sublevel	$\Delta E_{S_0 \leftarrow T_{1,\zeta}}$	$\lvert\mu_{el}(S_0 \leftarrow T_{1,\zeta})\rvert$	$\Gamma_{1,\zeta}$	$\tau_{P,\zeta}$
$T_{1,a}$	12 524.1	$4.30 \times 10^{-6}(z)$	7.36×10^{-5}	1.36×10^4
$T_{1,b}$	12 524.1	—	—	—
$T_{1,c}$	12 524.1	$2.24 \times 10^{-4}(y)$	2.00×10^{-1}	5.01
	High temperature average	—	6.66×10^{-2}	4.53×10^3

4. Summary and conclusions

The aim of the present work was to study the possible intersystem crossing (ISC) channels that could promote efficient singlet–triplet ISC in photoexcited thionine. To this end, the ISC rate constants have been computed for the adiabatically accessible triplet state population mechanisms and a qualitative interpretation of the photophysics is presented.

Irradiation of thionine with visible light will populate primarily the first excited singlet state $S_1(\pi_H \rightarrow \pi_L^*)$. At the $S_1(\pi_H \rightarrow \pi_L^*)$ minimum only the first two triplet states T_1 and $T_2(\pi \rightarrow \pi^*)$ are energetically accessible. Their electronic spin–orbit coupling (SOC) matrix elements with the $S_1(\pi_H \rightarrow \pi_L^*)$ state nearly vanish. Since the direct SOC does not explain the high triplet quantum yield in this system, we focused on the ISC driven by vibronic SOC. In a vacuum, the $S_1(\pi_H \rightarrow \pi_L^*) \rightsquigarrow T_2(\pi_{H-1} \rightarrow \pi_L^*)$ ISC channel was found to efficiently proceed with an ISC rate constant of $k_{ISC} \approx 3 \times 10^8$ s^{-1}, well able to compete with fluorescence from the $S_1(\pi_H \rightarrow \pi_L^*)$ state ($k_F \approx 2 \times 10^8$ s^{-1}). The $S_1(\pi_H \rightarrow \pi_L^*) \rightsquigarrow T_1(\pi_H \rightarrow \pi_L^*)$ ISC channel was estimated to be less efficient ($k_{ISC} \approx 10^5$–10^6 s^{-1}). The higher efficiency of the $S_1(\pi_H \rightarrow \pi_L^*) \rightsquigarrow T_2(\pi_{H-1} \rightarrow \pi_L^*)$ ISC channel originates on the one hand due to a more pronounced vibronic SOC, arising from the presence of the high electron density at the sulphur center in the π_{H-1} molecular orbital. This in turn induces a more effective mixing with the n molecular orbital upon elongations along certain *out-of-plane* vibrational normal modes. On the other hand, the accessibility of this channel is promoted by more favourable Franck–Condon factors, evidenced by the presence of a crossing between the S_1 and $T_2(\pi \rightarrow \pi^*)$ states.

Due to the near degeneracy of the adiabatic $S_1(\pi_H \rightarrow \pi_L^*)$ and $S_2(\pi_{H-1} \rightarrow \pi_L^*)$ minima and the nearby barrierless conical intersection, a small population of the dark $S_2(\pi_{H-1} \rightarrow \pi_L^*)$ state might be thought to be plausible. However, transitions starting from the $S_2(\pi_{H-1} \rightarrow \pi_L^*)$ to the T_1 and $T_2(\pi \rightarrow \pi^*)$ states are not realistic candidates for efficient ISC channels as the calculated rates are of the order of $\approx 10^6\ s^{-1}$.

The effect of water as a solvent on the ISC rates was also studied. Based on our results, we propose that the efficient triplet quantum yield of thionine in water is primarily due to the $S_1(\pi_H \rightarrow \pi_L^*) \rightsquigarrow T_2(\pi_{H-1} \rightarrow \pi_L^*)$ channel with a computed rate constant of the order of $\approx 10^8$–$10^9\ s^{-1}$ which agrees well with the experimental finding ($k_{ISC} = 2.8 \times 10^9\ s^{-1}$).[19] The ratio of the calculated ISC rate constant $\approx 10^9\ s^{-1}$ to the fluorescence rate constant which is of the order of $10^8\ s^{-1}$ is also consistent with the measured lower fluorescence ($\phi_F \approx 0.1$–0.027)[15–17] and sizeable triplet quantum yields ($\phi_T = 0.55$)[12] in water. We can therefore conclude that the experimentally observed triplet quantum yield is mainly due to the $S_1(\pi_H \rightarrow \pi_L^*) \rightsquigarrow T_2(\pi_{H-1} \rightarrow \pi_L^*)$ ISC channel which is driven by vibronic SOC.

Acknowledgements

Financial support from Fundación para la Promoción de la Ciencia y la Tecnología del Banco de la República (Project 2630), Universidad Industrial de Santander (Project 5169) and Deutsche Forschungsgemeinschaft through MA 1052/12-1 is gratefully acknowledged. A. Rodriguez-Serrano thanks COLCIENCIAS 'Programa generación bicentenario, becas Francisco José de Caldas'.

References

1 K. M. Gangotri and R. C. Meena, Use of reductant and photosensitizer in photogalvanic cells for solar energy conversion and storage: oxalic acid–methylene blue system, *J. Photochem. Photobiol.*, 2001, 141–175.
2 C. Lal, Use of mixed dyes in a photogalvanic cell for solar energy conversion and storage: EDTA–thionine–azur-B system, *J. Power Sources*, 2004, **164**, 926.
3 F. Harris, Z. Sayed, S. Hussain and D. A. Phoenix, An investigation into potential of phenothiazinium-based photo-sensitisers to act as PDT agents, *Photodiagn. Photodyn. Ther.*, 2004, **1**, 231.
4 J. P. Tardivo, A. Del Giglio, C. Santos de Oliveira, D. Santesso Gabrielli, H. Couto Junqueira, D. Batista Tadab, D. Severino, R. de Fatima Turchiello and M. S. Baptista, Methylene blue in photodynamic therapy: from basic mechanisms to clinical applications, *Photodiagn. Photodyn. Ther.*, 2005, **2**, 175.
5 E. M. Tuite and J. M. Kelly, Photochemical reactions of methylene blue and analogues with DNA and other biological substrates, *J. Photochem. Photobiol., B*, 1993, **21**, 103.
6 H. E. A. Kramer and A. Maute, Sensitized photooxygenation according to type I mechanism (radical mechanism) – part I. Flash photolysis experiments, *Photochem. Photobiol.*, 1972, **15**, 7.
7 D. R. Kearns, Physical and chemical properties of singlet molecular oxygen, *Chem. Rev.*, 1971, **71**, 395.
8 A. Rodriguez-Serrano, M. C. Daza, M. Doerr and C. M. Marian, A quantum chemical investigation of the electronic structure of thionine, *Photochem. Photobiol. Sci.*, 2012, **11**, 397.
9 F. Furche and R. Ahlrichs, Adiabatic time-dependent density functional methods for excited state properties, *J. Chem. Phys.*, 2002, **117**, 7433.
10 S. Grimme and M. Waletzke, A combination of Kohn–Sham density functional theory and multi-reference configuration interaction methods, *J. Chem. Phys.*, 1999, **111**, 5645.
11 L. F. Epstein, F. Karush and E. Rabinowitch, A spectrophotometric study of thionine, *J. Opt. Soc. Am.*, 1941, **31**, 77.
12 M. Nemoto, H. Kokubun and M. Koizumi, Determination of S*–T transition probabilities of some xantene and thiazine dyes on the basis of T-energy transfer. II. Results in the aqueous solution, *Bull. Chem. Soc. Jpn*, 1969, **42**(1223), 2464.
13 M. G. Neumann and M. J. Tiera, The use of basic dyes as photochemical probes, *Química Nova*, 1993, **16**(4), 280.
14 S. Das and P. V. Kamat, Can H-aggregates serve as light-harvesting antennae? Triplet–triplet energy transfer between excited aggregates and monomer thionine in aersol-OT solutions, *J. Phys. Chem. B*, 1999, **103**, 209.
15 E. Rabinowitch and L. F. Epstein, Polymerization of dyestuffs in solution. Thionine and methylene blue, *J. Am. Chem. Soc.*, 1941, **63**, 69.
16 G. R. Haugen and E. R. Hardwick, Ionic association in aqueous solutions of thionine, *J. Phys. Chem.*, 1963, **67**, 725.
17 G. R. Haugen and E. R. Hardwick, Ionic association in solutions of thionine. II. Fluorescence and solvent effects, *J. Phys. Chem.*, 1965, **69**, 2988.
18 M. D. Archer, M. I. C. Ferreira, G. Porter and C. J. Tredwell, Picosecond study of Stern–Volmer quenching of thionine by ferrous ions, *Nouv. J. Chim.*, 1977, **1**, 9.
19 U. Steiner, G. Winter and H. E. A. Kramer, Investigation of physical triplet quenching by electron donors, *J. Phys. Chem.*, 1977, **81**, 1104.
20 S. K. Lower and M. A. El-Sayed, The triplet state and molecular electronic processes in organic molecules, *Chem. Rev.*, 1966, **66**, 199.
21 J. Tatchen, N. Gilka and C. M. Marian, Intersystem crossing driven by vibronic spin–orbit coupling: a case study on psoralen, *Phys. Chem. Chem. Phys.*, 2007, **9**, 5209.
22 S. Salzmann, J. Tatchen and C. M. Marian, The photophysics of flavins: What makes the difference between gas phase and aqueous solution?, *J. Photochem. Photobiol., A*, 2008, **198**, 221.
23 S. Perun, J. Tatchen and C. M. Marian, Singlet and triplet excited states and intersystem crossing in free-base porphyrin: TDDFT and DFT/MRCI study, *ChemPhysChem*, 2008, **9**, 282.
24 A. D. Becke, Density-functional thermochemistry. III. The role of exact exchange, *J. Chem. Phys.*, 1993, **98**, 5648.
25 P. A. M. Dirac, Quantum mechanics of many-electron systems, *Proc. R. Soc. London, Ser. A*, 1929, **123**, 714.
26 A. Schäfer, C. Huber and R. Ahlrichs, Fully optimized contracted Gaussian basis sets of triple zeta valence quality for atoms Li to Kr, *J. Chem. Phys.*, 1994, **100**, 5829.
27 TURBOMOLE V6.3 2011, a development of University of Karlsruhe and Forschungszentrum Karlsruhe GmbH, 1989–2007, TURBOMOLE GmbH, since 2007; available from http://www.turbomole.com
28 C. Kind, M. Reiher and J. Neugebauer, *SNF Version 2.2.1: A Program Package for Numerical Frequency Analyses*, Universität Erlangen, 1999–2002.
29 J. Tatchen, *Spin-verbotene photophysikalische Prozesse in organischen Molekuelen: Entwicklung quantenchemischer Methoden und Anwendung auf Psoralene*, PhD thesis, Universität Düsseldorf, Germany, 2005.
30 P. A. M. Dirac, The quantum theory of the emission and absorption of radiation, *Proc. R. Soc. London, Ser. A*, 1927, **114**, 243.
31 G. Wentzel, Über strahlungslose Quantensprünge, *Z. Phys.*, 1927, **43**, 524.
32 M. Kleinschmidt, J. Tatchen and C. M. Marian, Spin–orbit coupling of DFT/MRCI wavefunctions: method, test calculations, and application to thiophene, *J. Comput. Chem.*, 2002, **23**, 824.
33 M. Kleinschmidt and C. M. Marian, Efficient generation of matrix elements for one-electron spin–orbit operators, *Chem. Phys.*, 2005, **311**, 71.
34 M. Kleinschmidt, J. Tatchen and C. M. Marian, SPOCK.CI: a multireference spin–orbit configuration interaction method for large molecules, *J. Chem. Phys.*, 2006, **124**, 124101.
35 B. A. Heß, C. M. Marian, U. Wahlgren and O. Gropen, A mean-field spin–orbit method applicable to correlated wavefunctions, *Chem. Phys. Lett.*, 1996, **251**, 365.
36 N. J. Turro, V. Ramamurthy and J. C. Scaiano, *Principles of Molecular Photochemistry: An Introduction*, University Science Books, Sausalito, CA, 2009.

